Proceedings of the ASME 2024
ICE Forward Conference
ICEF2024
October 20-23, 2024, San Antonio, Texas

ICEF2024-138846

A MINIMUM AREA PISTON FOR COMPRESSION IGNITION ENGINES

Felix Leach*, Martin Davy
University of Oxford
Oxford, UK
* felix.leach@eng.ox.ac.uk

Sridhar Ayyapureddi, Steven Pierson, Juan San Primitivo Rodriguez, Gilbert Sammut
JLR
Coventry, UK

ABSTRACT

Conventional compression ignition (diesel) engine combustion system, employ pistons with omega shaped bowls (or a very similar shape) combined with a swirl-based bulk air motion to ensure good fuel-air mixing. However, such bowls have a relatively large surface area:volume ratio, leading to significant heat loss, and are complex to design and manufacture. Recent advances in fuel injection technology, allowing higher injection pressures and multiple injection events and digital rate shaping, along with variable intake valve technology mean that achieving sufficient fuel-air mixing may now not require an omega shaped bowl. This work, then, introduces a new piston design for compression ignition engines that minimises the surface area:volume ratio, enabling less heat loss through the piston, higher durability, and a lighter and easier to produce piston.

This novel piston design is evaluated against a conventional (omega) bowl piston (maintaining compression ratio and other parameters) at a variety of part and full load conditions in a single cylinder research engine. Emissions, fuel consumption, and combustion parameters are measured and presented alongside an energy balance. The results show that, depending on the load conditions, a 1.5-4% decrease in fuel consumption is noted alongside, at some load conditions, an increase in exhaust temperature (providing extra enthalpy for a turbocharger). The energy balance showed less energy lost to the oil with more energy in the exhaust.

INTRODUCTION

Diesel engines remain an important part of the transportation system, notably in the heavy-duty, off-highway, and marine sectors but also, in lesser quantities, in the light-duty sector – particularly for applications which require higher torque. Ever-tightening regulation motivated by important concerns about climate change has led to increased efforts to improve diesel engine efficiency [1, 2]. In diesel engines, heat losses to oil and coolant account for up to 45% of total energy losses (in terms of input fuel energy), depending on operating conditions [3-5].

Recent strategies for reducing these heat losses from diesel engines and improving their efficiency include use of piston materials such as steel, which thanks to its lower thermal conductivity, can reduce heat transfer to oil and coolant (amongst other benefits including higher strength – leading to lighter weight pistons, lower thermal expansion, shorter piston skirts, and lower conrod forces) [6, 7]. Surface coatings such as ceramics have also been considered due to their substantially lower thermal conductivity, including early attempts at so-called adiabatic engines [8, 9], which suffered from low volumetric efficiencies. More recent work has focused on so-called ‘active’ thermal coatings, which are designed to allow the surface temperatures of the combustion chamber surfaces to follow the gas temperature and hence reduce the heat losses [10-12].

Diesel engines typically use an omega shaped combustion bowl, which promote air-fuel mixing at fuel injection through a swirl based bulk air motion combustion system design [13-15]. Some studies have shown that adding a ramp, or lip, to this bowl can have a significant influence on the emissions formation from combustion thanks to the detail of the air-fuel mixing [16-19]. However, omega shaped bowls have high surface area to volume ratios, which means that the potential for heat losses through the piston is high and they are complex to design and manufacture. This trade-off between good air-fuel mixing for better combustion and lower emissions and higher heat losses has been fairly settled in recent times.

Recent advances in digital fuel injection technology, including piezoelectric fuel injectors and high fuel injection system pressures along with variable intake valve technology, have enabled much more comprehensive control of the air-fuel mixing through the fuel injection and valvetrain systems rather than through the air motion by having multiple fuel injections (say up to eight) within a single engine cycle – often referred to as digital rate shaping [20-24].

Such advances, therefore, beg the question: is the omega bowl shape (or its variants) still necessary to ensure sufficient air-fuel mixing or can digital rate shaping now provide sufficient air-fuel mixing to enable a radically different combustion bowl design aimed at reducing heat losses? This paper aims to explore that question by introducing a new piston design - based on minimising the surface area to volume ratio enabling less heat loss through the piston as well as higher durability, and a lighter and easier to produce piston.

METHODOLODGY

The design of the piston was motivated by the desire to minimize its surface area – to develop a Minimum Area Piston (MAP). The final shape chosen is shown in Figure 1 labelled as MAP. This shows, in addition, the conventional omega piston design, alongside a simple parabola design, which would minimize the surface area to volume ratio as much as possible as well as an indication of the fuel spray targeting from the injector. The design that was chosen, MAP, was chosen so that the air fuel mixing could be maximized by minimizing the space directly beneath the fuel injector which fuel is not injected directly into, where air-fuel mixing would be challenging to achieve. However, outside of this region the MAP design follows the simple parabola shape and is designed to retain the same compression ratio as the original omega bowl. A patent has been filed to protect these piston designs [25].

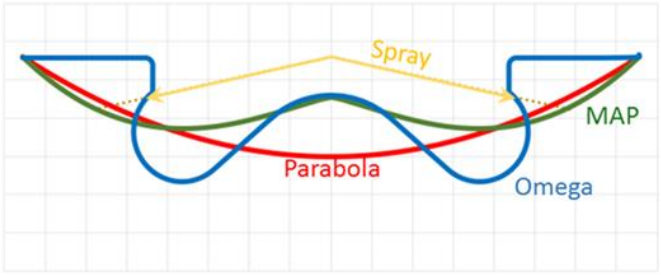

FIGURE 1: COMPARISON BETWEEN OMEGA AND MAP BOWLS USED IN THIS WORK

Both the MAP piston and the baseline (omega) piston were tested in a single-cylinder direct injection diesel engine. The engine configuration and its peripherals have been described in detail in previous publications [14, 26]. A split cooling system was employed whereby the cylinder head and cylinder jacket temperatures can be controlled independently. A piston cooling jet was also employed to reduce the operating temperature of the piston. Further details of the engine are shown in Table 1.

Cylinder pressure data was measured using a high-speed piezoelectric Kistler 6046Asp-3-2 transducer. The pressure signal was recorded at 0.1 CAD resolution using an AVL Indicom high-speed data acquisition system. Corresponding high-speed data was recorded for engine shaft encoder position. These high-speed signals were subsequently used to calculate the heat release and mass fraction burned (MFB) between the limits of -25 and 135 CAD using the standard packages available within the AVL Concerto software. Low frequency channels were logged at 1 Hz using the facility's Sierra-CP engineering. CADET engine control system.

TABLE 1: ENGINE PARAMETERS

Displacement / cylinder	500 cm^3
Bore × Stroke	83mm × 92.4mm
Valves per cylinder	2 intake, 2 exhaust
EVO	128 °atdcf
EVC	382 °atdcf
Fuel pressure	2200 bar maximum
Injector type	8-hole solenoid

Fuel flow measurements were carried out using both a gravimetric (Sierra-CP FuelTrak 1000) and a coriolis fuel flow meter (Siemens SITRANS F C MASSFLO MASS2100). The agreement between the two flow meters was within 1 % even at the very low flow rates associated with low-load single-cylinder operation. A Horiba MEXA-ONE emissions analyser was employed for gaseous emissions measurements with an AVL-415S smoke meter being used for smoke measurement. The small coolant temperature differences across the engine were measured using a high-accuracy differential thermocouple system developed in a previous work [3], The mean exhaust gas temperature, and all other system temperatures around the engine were measured using standard 3 mm k-type thermocouples [27, 28].

The engine was operated at three different speed and load conditions designed to be representative of the engine operating map as shown in Table 2. A five-point Exhaust Gas Recirculation (EGR) sweep was performed for the first two conditions so as to minimize NO_x emissions – a smoke limit of approximately 3 FSN being applied to determine the maximum EGR rate. Test point three was a full load test point, full load was defined as the point of maximum load limited by peak cylinder pressure and peak exhaust temperature; no EGR was run at this point. For all test points, the angle of 50 % mass fraction burned (CA50) was held constant via a closed-loop control of fuel injection timing.

The coolant and oil inlet temperatures and the intake air temperatures were held constant at the values shown in Table 2 by external conditioning systems. To provide adequate data for robust statistical analysis a minimum of two repeats were performed for each EGR point (for a total of at least three runs) with the 1 Hz data logged for three minutes and the 0.1 CAD data logged for 300 cycles. All error bars presented in this work then indicate one standard deviation over a three-minute log for the low-speed data or 300 cycles for the high-speed data. An EN590 compliant diesel fuel, with no oxygenate components present [29] from a single batch was used for all tests. For reasons of commercial confidentiality all emissions and fuel consumption results presented in this work have been rescaled by dividing by a nominal value – the same nominal value for all load points and as a result are presented as dimensionless. In addition, where results present NO_x, it is defined as $NO + NO_2$.

TABLE 2: TEST POINTS

Test point	1	2	3
Engine speed (rpm)	1500	2500	4000
nIMEP (bar)	3.8	17.7	Max
Exhaust back pressure (barG)	0.31	2.7	2.5
Inlet air temperature (°C)	55	40	50
Coolant and oil temperature (°C)	90	90	90
Fuel injection pressure (MPa)	58	147	220
Peak EGR (%)	52*	26*	0

*EGR was swept between this value and 0% in five equal steps.

Energy balance analysis

The energy balance analysis employs a control volume approach (CV on Figure 2) where the energy inputs to the control volume comprise; the fuel chemical energy, the enthalpy of intake air, the enthalpy of the EGR gases and the heat supplied by the oil sump heaters (note that results are presented as a fraction of this *total* input energy, Q_{in}). The measured or calculated energy out terms from the control volume are: the energy to the oil (Q_{oil}), brake efficiency (Brk. Eff.), energy to the coolant at the cylinder jacket (Q_{cool_jck}) and at the cylinder head (Q_{cool_head}), exhaust enthalpy (Q_{exh}), exhaust chemical energy (Q_{chem}), ancillaries (which on this engine is the fuel pump), and a term for extraneous losses (Q_{ext}), which lumps together all of the unaccounted energy terms and is high for this engine because this is a single cylinder engine with a very high surface area to cylinder ratio. The extraneous losses are dominated by convective and radiative heat transfers from these hot surfaces of the engine to the ambient air. Because this is 1st law energy analysis, all terms, whether heat energy or useful work, are treated the same. All terms are presented as normalised values to the total energy input for the baseline omega bowl piston. All error bars presented for the energy balance results indicate one standard deviation over the three repeats. The energy balance model is discussed in more detail in previous work [3].

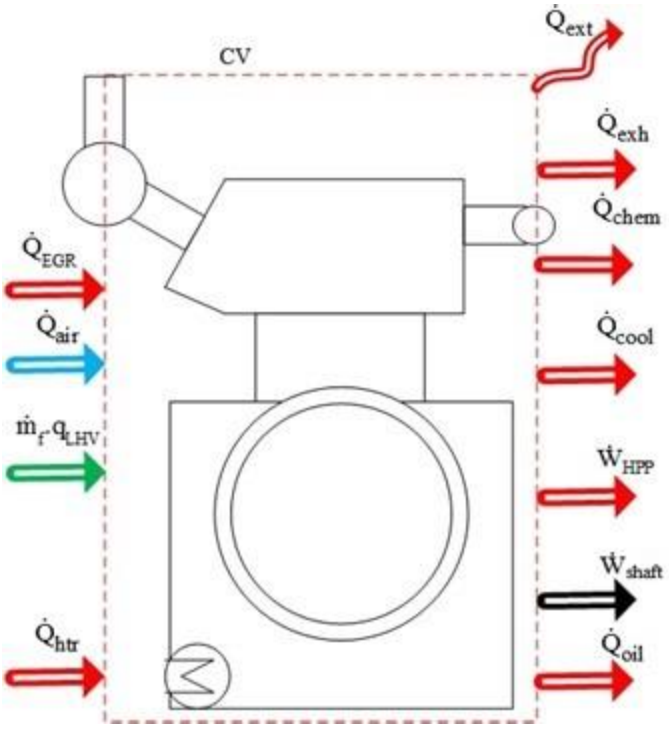

FIGURE 2: CONTROL VOLUME FOR THE ENERGY BALANCE MODEL. THE INPUTS TO THE MODEL ARE ON THE LEFT AND THE OUTPUTS ON THE RIGHT (ADAPTED FROM [3])

RESULTS

In this section, results are presented across the EGR sweeps conducted at the part load test points (TP1&2), which is represented by the varying net indicated specific NO_x ($ISNO_x$) emissions on the x-axis. On many figures, the different shapes (diamond, triangle, etc) represent a different, independent, test run, whereas the shading represents the baseline (solid) and MAP (hollow) bowls.

Light load

This section presents the results for the light load test condition, TP1, which is 1500 rpm / 3.8 bar nIMEP. Figure 3 presents the rescaled net indicated specific fuel consumption (ISFC) results – in this case a measured by the coriolis flow meter. At this test condition, roughly a 4% lower ISFC is observed for equivalent $ISNO_x$ emissions, with the highest reductions in ISFC seen at the highest EGR levels. It is worth observing that such a reduction in ISFC is amongst the highest difference that the authors have observed in conducting a lot of work on this engine (whether varying piston material, air flow, using thermal swing coatings or other efforts to reduce ISFC) [7, 12, 14, 19, 30].

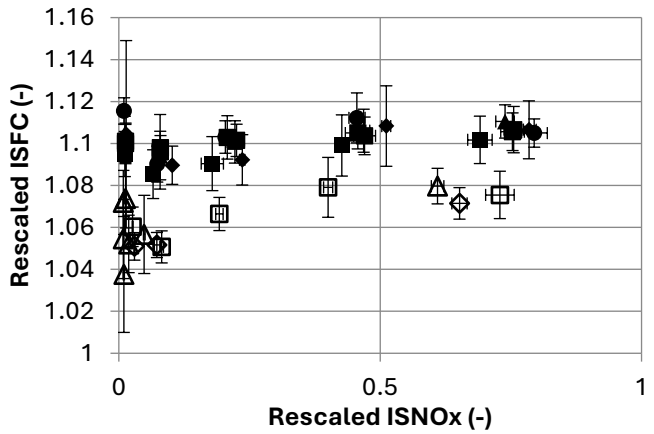

FIGURE 3: RESCALED $ISNO_X$-ISFC RESULTS FOR TP1. SOLID MARKERS ARE THE BASELINE (OMEGA BOWL) TEST POINTS AND HOLLOW ONES THE MAP. THE ERROR BARS INDICATE ± σ

Figure 4 shows the measured exhaust temperatures across the EGR sweep with the baseline (omega) piston and the MAP. It can clearly be seen that there is a 10-15°C increase in exhaust temperature observed across the EGR range with, again, the highest increases observed at the highest EGR (lowest $ISNO_x$) conditions. It should be noted that the injection strategies are exactly the same between the two pistons here, so the changes observed must be due to the differences in piston geometry. However, changes in injection strategy (either advancing or retarding the injections) could effectively be used to trade-off the ISFC improvements seen in Figure 3 and the exhaust temperature improvements seen in Figure 4 at this test condition. This increase in exhaust temperature should correspond to an increase in enthalpy in the exhaust available to the turbocharger.

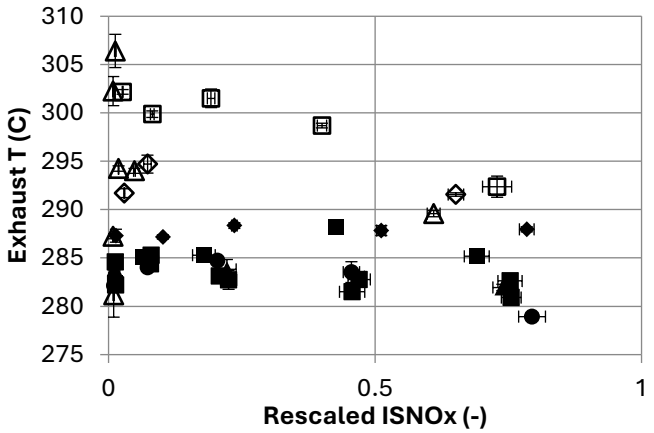

FIGURE 4: RESCALED $ISNO_X$-EXHAUST TEMPERATURE RESULTS FOR TP1. SOLID MARKERS ARE THE BASELINE (OMEGA BOWL) TEST POINTS AND HOLLOW ONES THE MAP. THE ERROR BARS INDICATE ± σ

The energy balance for this speed load site is shown in Figure 5. As this point is very low load, the engine requires external heating to maintain the operating temperatures, indicated by the negative numbers for the energy flows in the oil and coolant. The larger total energy input with the MAP at this point (9.9% of total compared to 8.2%) indicates a lower overall heat rejection to the coolant and oil. It should be noted however, the energy required to maintain the oil temperature is lower on the MAP than the baseline omega bowl indicating that, at this speed load site, the heat rejected to the piston is higher with the MAP than with the baseline omega bowl. The higher exhaust temperatures already seen in Figure 4 are reflected in the 2.2 percentage point (~10%) increase in total heat energy rejected in the exhaust with the MAP.

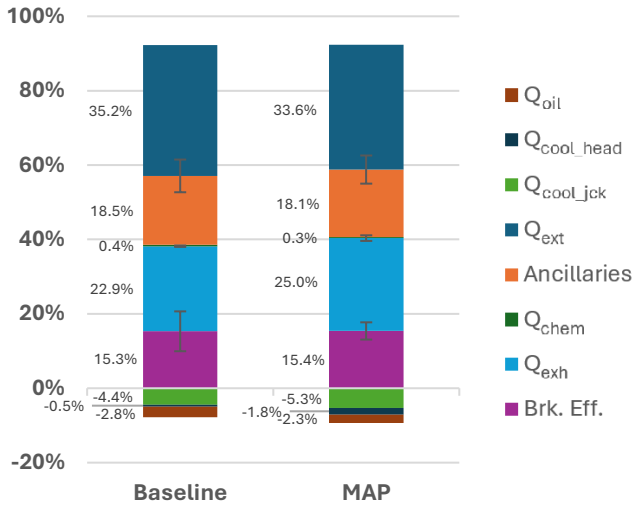

FIGURE 5: FIRST LAW ANALYSIS RESULTS FOR TP1 (0% EGR). RESULTS PRESENTED AS PERCENTAGE OF TOTAL ENERGY INPUT. THE ERROR BARS INDICATE ± σ

Figure 6 shows the NO_x-soot tradeoff for the MAP against the baseline piston. As might be expected, given the anticipated poorer air-fuel mixing, at this test condition, the soot emissions are higher for the MAP. However, the highest increases are seen at the mid-high EGR levels, before entering the Low Temperature Combustion (LTC) – high EGR – region, where low levels of soot emissions are seen with both pistons. In addition, it should be noted that the fuel injection strategy is the same between both test points and it is hoped that some of this soot increase can be recovered by incorporating split injection strategies to promote air-fuel mixing in the future.

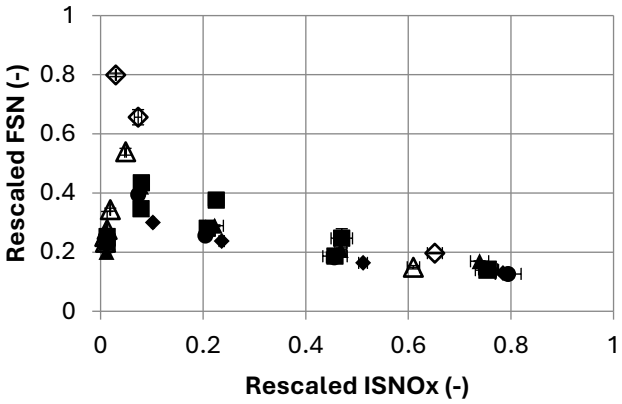

FIGURE 6: RESCALED ISNO$_X$-SOOT RESULTS FOR TP1. SOLID MARKERS ARE THE BASELINE (OMEGA BOWL) TEST POINTS AND HOLLOW ONES THE MAP. THE ERROR BARS INDICATE ± σ

Figure 7 shows the indicated specific total hydrocarbon (ISTHC) emissions results for the MAP and baseline piston. Across the EGR range, a 20-50% reduction in ISTHC emissions is observed with the MAP. It is thought that this might be because the air motion at the edges of the piston is oriented away from the piston crevices – towards the cylinder head – and hence there is less opportunity for unburned fuel to become lodged in the crevices and so more of the fuel is being combusted. However, CFD analysis in the future will be needed to verify this.

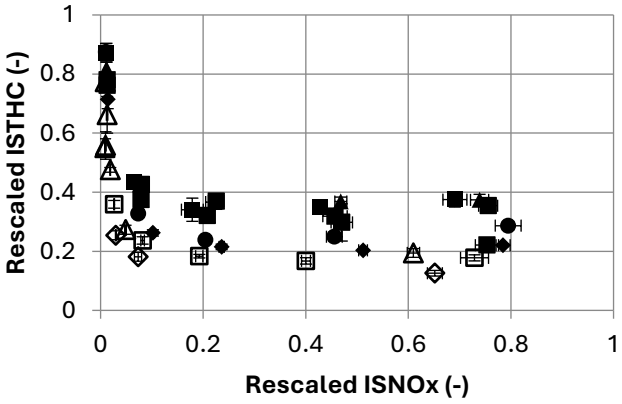

FIGURE 7: RESCALED ISNO$_X$-ISTHC RESULTS FOR TP1. SOLID MARKERS ARE THE BASELINE (OMEGA BOWL) TEST POINTS AND HOLLOW ONES THE MAP. THE ERROR BARS INDICATE ± σ

Medium load

This section presents the results for the light load test condition, TP2, which is 2500 rpm / 17.7 bar nIMEP. Figure 8 presents the rescaled net indicated specific fuel consumption (ISFC) results – again measured by the coriolis flow meter. In contrast to TP1, at this test condition, no noticeable difference in fuel consumption (ISFC) is observed anywhere across the ISNO$_x$ range.

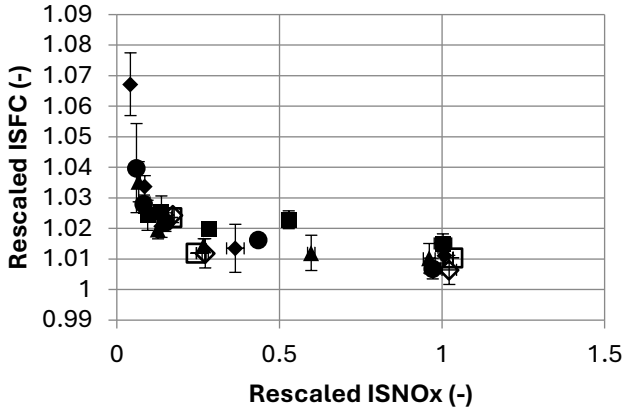

FIGURE 8: RESCALED ISNO$_X$-ISFC RESULTS FOR TP2. SOLID MARKERS ARE THE BASELINE (OMEGA BOWL) TEST POINTS AND HOLLOW ONES THE MAP. THE ERROR BARS INDICATE ± σ

Figure 9 shows the exhaust temperature results at TP2. At this test condition, in contrast to TP1, a small reduction (5-10°C) in exhaust temperature is seen across the ISNO$_x$ range. It seems that, at this condition, there is more heat transfer to the piston and combustion chamber surfaces and less to the exhaust.

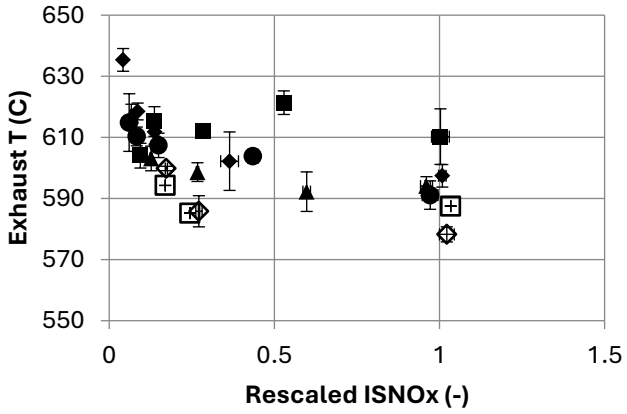

FIGURE 9: RESCALED ISNO$_X$-EXHAUST TEMPERATURE RESULTS FOR TP2. SOLID MARKERS ARE THE BASELINE (OMEGA BOWL) TEST POINTS AND HOLLOW ONES THE MAP. THE ERROR BARS INDICATE ± σ

The first law energy balance of this test condition is shown in Figure 10. As with TP1, all the values have been normalised to account for the different energy inputs (i.e. any variations in fuel consumption seen still sum to 100% here). With the MAP bowl, the brake thermal efficiency is reduced 3 percentage points, and the exhaust gas energy is reduced by 1.1 percentage

points (corresponding to the reductions in exhaust temperature seen in Figure 9). It is not immediately clear why this is, but it may be that . The heat rejection to the oil has been reduced with MAP by 1.1 percentage points, showing the reduced surface area has resulted in lower heat rejection through the piston. The head and block coolant heat rejection rates are increased by 1.6 percentage points and 1.1 percentage points respectively.

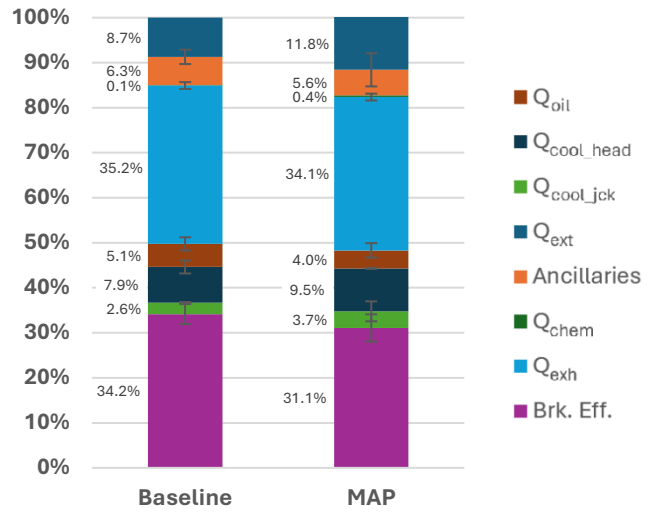

FIGURE 10: FIRST LAW ANALYSIS RESULTS FOR TP2 (0% EGR). RESULTS PRESENTED AS PERCENTAGE OF TOTAL ENERGY INPUT. THE ERROR BARS INDICATE ± σ

Figure 11 shows the NO_x-soot tradeoff for the MAP against the baseline piston. As was seen with TP1, there is an increase in soot emissions seen with the MAP, again, this is likely due to the poorer air-fuel mixing that is expected with the MAP.

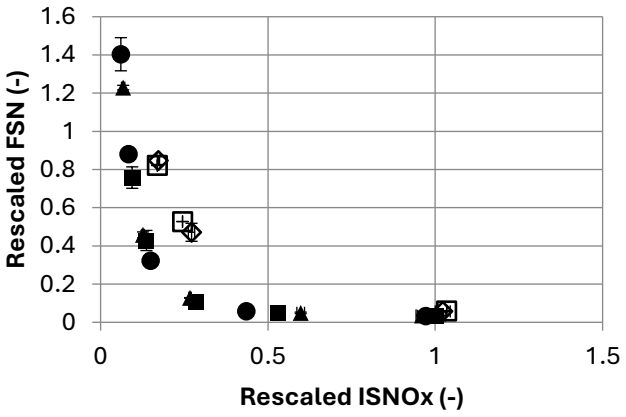

FIGURE 11: RESCALED $ISNO_X$-SOOT RESULTS FOR TP2. SOLID MARKERS ARE THE BASELINE (OMEGA BOWL) TEST POINTS AND HOLLOW ONES THE MAP. THE ERROR BARS INDICATE ± σ

Figure 12 shows the ISTHC emissions at TP2. Similarly to TP1, the THC emissions are slightly reduced with the MAP, compared to the baseline (omega) piston. Again, this is thought to be due to the air motion in the cylinder near the crevices, which keeps unburned fuel out of the crevices.

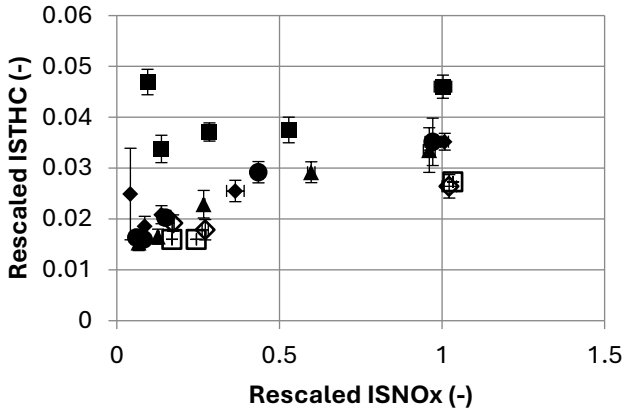

FIGURE 12: RESCALED $ISNO_X$-ISTHC RESULTS FOR TP2. SOLID MARKERS ARE THE BASELINE (OMEGA BOWL) TEST POINTS AND HOLLOW ONES THE MAP. THE ERROR BARS INDICATE ± σ

Given the difference in fuel consumption performance of the MAP between TP1 and TP2, the combustion characteristice were investigated at this test condition. Figure 13 shows the burn duration (MFB10-90%) and Figure 14 shows the ignition delay comparision between the MAP and the baseline at TP2. No significant difference in burn duration is observed between the MAP and the baseline which, whilst not helping to explain the difference in fuel consumption, is interesting given the substantially different air-fuel mixing that will be taking place in the MAP compared to the baseline. However, the substantial increase in ignition delay (Figure 14) with the MAP may well explain some of the decrease in efficiency seen at this operating point, although the main combustion duration is similar, the fuel is needing to be injected earlier (to maintain the MFB50) and the poorer fuel-air mixing with the MAP is leading to the increased ignition delay and hence decreased efficiency.

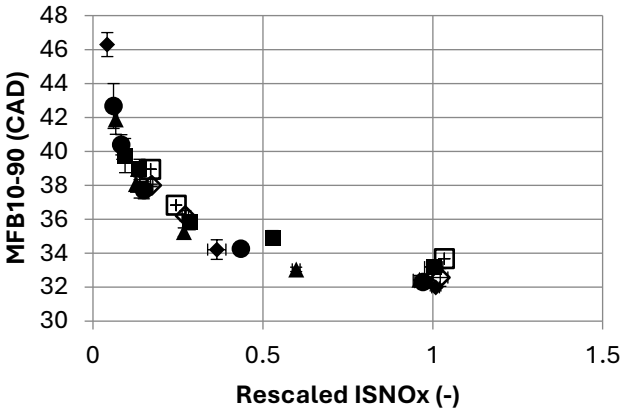

FIGURE 13: RESCALED ISNO$_X$-BURN DURATION (MFB10-90) RESULTS FOR TP2. SOLID MARKERS ARE THE BASELINE (OMEGA BOWL) TEST POINTS AND HOLLOW ONES THE MAP. THE ERROR BARS INDICATE ± σ

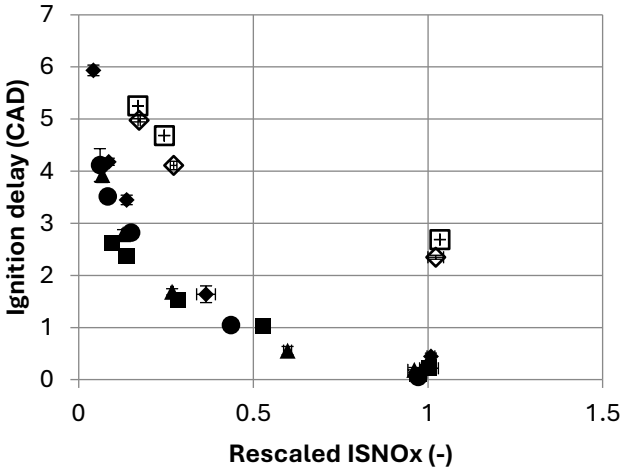

FIGURE 14: RESCALED ISNO$_X$-IGNITION DELAY (MSOI-MFB10) RESULTS FOR TP2. SOLID MARKERS ARE THE BASELINE (OMEGA BOWL) TEST POINTS AND HOLLOW ONES THE MAP. THE ERROR BARS INDICATE ± σ

Full load

As noted above, full load was limited by peak cylinder pressure and peak exhaust temperature rather than being a fixed value (i.e. unlike TP1 and TP2, the exhaust temperature and peak cylinder pressure are held constant at this test point). Hence the load of the engine can change at this test point. Figure 15 shows the nIMEPs reached at TP3. It can be seen that the MAP is giving a ~2.5% increase in peak power compared to the baseline (omega) piston. However, this increase in peak power has come with the penalty of slightly higher engine-out NO_x emissions (remember no EGR was run at this point to control NO_x). This indicates that there is slightly more fuel being injected (given the constraints of peak cylinder pressure and maximum exhaust temperature) at this speed and load, leading to overall hotter combustion, hence the increase in both IMEP and NO_x. This NO_x could be controlled either with EGR or with aftertreatment such as SCR.

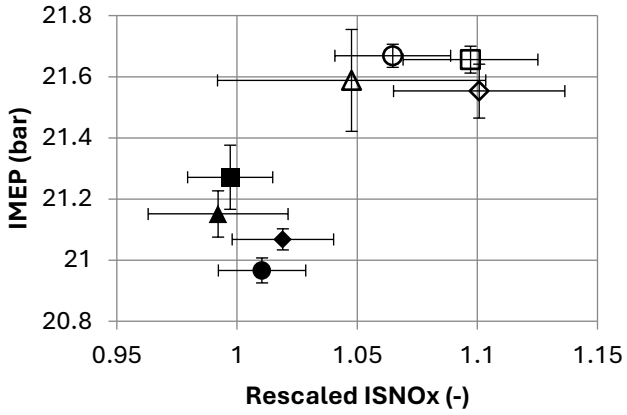

FIGURE 15: RESCALED ISNO$_X$-IMEP RESULTS FOR TP3. SOLID MARKERS ARE THE BASELINE (OMEGA BOWL) TEST POINTS AND HOLLOW ONES THE MAP. THE ERROR BARS INDICATE ± σ

The fuel consumption results at TP3 are shown in Figure 16. Similar to TP1, a 3-5% lower ISFC is observed here with the MAP compared to the baseline piston. The authors again observe that this is a substantial improvement in fuel consumption that is notably higher than that available with significant other changes to this diesel engine in previous work.

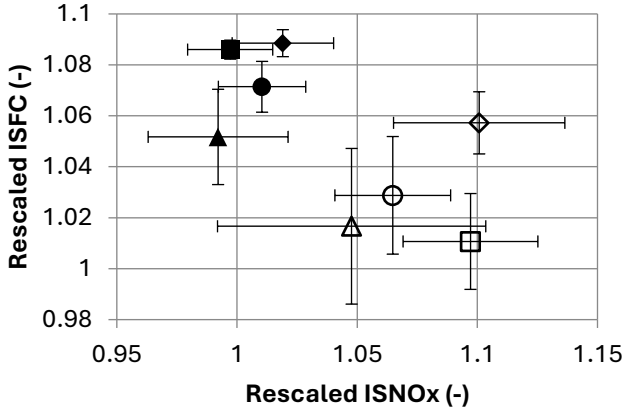

FIGURE 16: RESCALED ISNO$_X$-ISFC RESULTS FOR TP3. SOLID MARKERS ARE THE BASELINE (OMEGA BOWL) TEST POINTS AND HOLLOW ONES THE MAP. THE ERROR BARS INDICATE ± σ

Figure 17 shows the burn durations (MFB10-90%) for the MAP and the baseline at TP3. As at TP2, no significant difference in burn duration is observed between the MAP and the

baseline at this full load test point – TP3 – either. Considering ignitin delay (not shown here for brevity), there is an approximately 15% increase in ignition delay for the MAP.

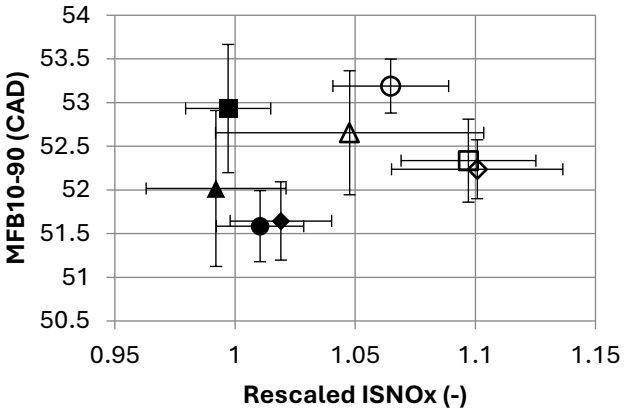

FIGURE 17: RESCALED ISNO$_X$-MFB10-90 RESULTS FOR TP3. SOLID MARKERS ARE THE BASELINE (OMEGA BOWL) TEST POINTS AND HOLLOW ONES THE MAP. THE ERROR BARS INDICATE ± σ

Figure 18 shows the smoke emissions at TP3. Similar to all of the other points tested, a significant increase in smoke emissions is observed with the MAP – indicative of the poorer air-fuel mixing that is expected with the MAP. Future work will investigate fuel injection strategies to improve this mixing.

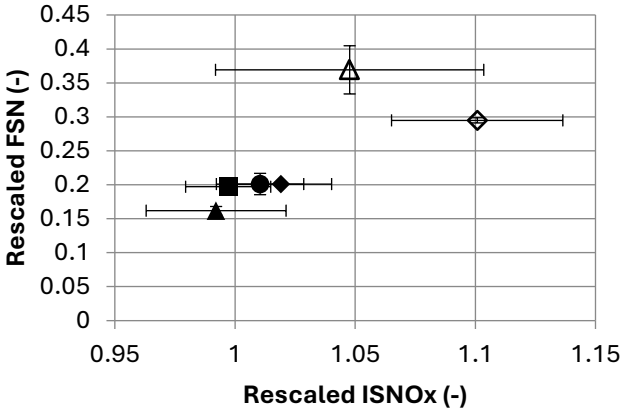

FIGURE 18: RESCALED ISNO$_X$-SOOT RESULTS FOR TP3. SOLID MARKERS ARE THE BASELINE (OMEGA BOWL) TEST POINTS AND HOLLOW ONES THE MAP. THE ERROR BARS INDICATE ± σ

CONCLUSIONS

In this work the effect of a minimum area piston (MAP) bowl on a high-speed direct injection diesel engine was investigated. The MAP bowl was compared against a reference omega shaped bowl piston over three engine test points and a range of EGR rates. Emissions, heat release and energy balance results showed that at light loads and low speed (TP1) the MAP bowl has shown a benefit compared to the baseline through reduced heat rejection to the piston resulting in higher exhaust gas temperatures and lower ISFC. The ISFC can be traded with exhaust gas temperature to achieve the lowest emissions to CO_2 emissions balance. This substantial improvement, however, comes at the expense of higher soot emissions, which is likely due to the poorer air-fuel mixing that is expected with the MAP.

At medium load and mid-speed (TP2), very few differences between the MAP and the baseline were observed.

However, at full load and maximum speed (TP3), again the MAP showed substantial benefits including a 2.5% increase in peak power and 3-5% improvement in ISFC. However, this, again, came with the penalty of increased soot emissions.

The authors note that the reduction in ISFC observed with the MAP at TP1 and TP3 is amongst the highest difference that the authors have observed in numerous different tests on this engine over the years – giving an indication of the potential for this novel piston design.

Future work focus on CFD modelling of the MAP design in order to understand the air-fuel interactions and experimental variation in fuel injection strategies combined with air motion studies in order to reduce the soot penalty observed with this piston, given its potential for substantial fuel consumption and exhaust enthalpy benefits.

NOMENCLATURE

atdcf	After top dead centre firing
CA50	Crank Angle of 50% mass fraction burned
CAD	Crank Angle Degree
CFD	Computational Fluid Dynamics
CV	Control Volume
ECU	Electronic Control Unit
EGR	Exhaust Gas Recirculation
EVC	Exhaust Valve Closing angle
EVO	Exhaust Valve Opening angle
FSN	Filter Smoke Number
IMEP	Indicated Mean Effective Pressure
ISFC	Indicated Specific Fuel Consumption
ISNO$_x$	Indicated Specific Oxides of Nitrogen
ISTHC	Indicated Specific Total Hydrocarbon
LTC	Low Temperature Combustion
nIMEP	net Indicated Mean Effective Pressure
nISFC	net Indicated Specific Fuel Consumption
MAP	Minimum Area Piston
MFB10-90	Duration of 10%-90% Mass Fraction Burned
NO$_x$	Oxides of Nitrogen
rpm	Revolutions per minute
SCR	Selective Catalytic Reduction
THC	Total Hydrocarbon
TPX	Test Point X

ACKNOWLEDGMENTS

The authors would like to thank JLR and the University of Oxford John Fell Fund for financial support. For the purpose of

 The authors would like to thank Nick Papaioannou and the Department of Engineering Science technicians and maintenance teams for undertaking much of the engine testing and facilities support. Holly Freed is thanked for help with data analysis. Lyn McWilliam is thanked for her extensive input into this work.

REFERENCES

1. Joshi, A., *Review of Vehicle Engine Efficiency and Emissions,* SAE Int. J. Adv. & Curr. Prac. in Mobility , 2022. **4**(5):1704-1733, https://doi.org/10.4271/2022-01-0540
2. Senecal, K. and F. Leach, *Racing Toward Zero: The Untold Story of Driving Green*. Warrendale, PA, USA: SAE International, 2021.
3. Papaiouannou, N., et al., *Evaluation of EGR techniques on a HSDI diesel engine using first law analysis.* Proceedings of the Institution of Mechanical Engineers, Part D: Journal of Automobile Engineering, 2018. **222**(3):710-726, https://doi.org/10.1177/0954407017749110
4. Smith, L., Preston, W., Dowd, G., Taylor, O. et al., *Application of a First Law Heat Balance Method to a Turbocharged Automotive Diesel Engine*, SAE Technical Paper 2009-01-2744, 2009, https://doi.org/10.4271/2009-01-2744
5. Heywood, J.B., *Internal combustion engine fundamentals*. Vol. 930. New York, NY, USA: Mcgraw-Hill, 1988.
6. Schreer, K., et al., *Analysis of Aluminum and Steel Pistons—Comparison of Friction, Piston Temperature, and Combustion.* Journal of Engineering for Gas Turbines and Power, 2014. **136**(10):101506, https://doi.org/10.1115/1.4027275
7. Papaioannou, N., Leach, F., and Davy, M., *Thermal Analysis of Steel and Aluminium Pistons for an HSDI Diesel Engine,* SAE Technical Paper 2019-01-0546, 2019, https://doi.org/10.4271/2019-01-0546
8. Osawa, K., Kamo, R., and Valdmanis, E., *Performance of Thin Thermal Barrier Coating on Small Aluminum Block Diesel Engine,* SAE Technical Paper 910461, 1991, https://doi.org/10.4271/910461
9. Kamo, R., *Adiabatic diesel-engine technology in future transportation.* Energy, 1987. **12**(10):1073-1080, https://doi.org/10.1016/0360-5442(87)90063-6
10. Caputo, S., Millo, F., Cifali, G., and Pesce, F., *Numerical Investigation on the Effects of Different Thermal Insulation Strategies for a Passenger Car Diesel Engine*, SAE Int. J. Engines, 2017. **10**(4):2154-2165, https://doi.org/10.4271/2017-24-0021
11. Somhorst, J., Uczak De Goes, W., Oevermann, M., and Bovo, M., *Experimental Evaluation of Novel Thermal Barrier Coatings in a Single Cylinder Light Duty Diesel Engine*, SAE Technical Paper 2019-24-0062, 2019, https://doi.org/10.4271/2019-24-0062
12. Papaioannou, N., Leach, F., Davy, M., and Gilchrist, R., *The Effect of an Active Thermal Coating on Efficiency and Emissions from a High Speed Direct Injection Diesel Engine*, SAE Technical Paper 2020-01-0807, 2020, https://doi.org/10.4271/2020-01-0807
13. Leach, F., R. Ismail, and M. Davy, *Engine-out emissions from a modern high speed diesel engine – The importance of Nozzle Tip Protrusion.* Applied Energy, 2018. **226**:340-352, https://doi.org/10.1016/j.apenergy.2018.05.117
14. Leach, F., Davy, M., Weall, A., and Cooper, B., *Comparing the Effect of a Swirl Flap and Asymmetric Inlet Valve Opening on a Light Duty Diesel Engine,* SAE Technical Paper 2017-01-2429, 2017, https://doi.org/10.4271/2017-01-2429
15. Miles, P.C. and Ö. Andersson, *A review of design considerations for light-duty diesel combustion systems.* International Journal of Engine Research, 2016. **17**(1):6-15, https://doi.org/10.1177/1468087415604754
16. Busch, S., F. Perini, and R.D. Reitz, *Light-Duty Diesel Combustion*, C.R.F. Sandia National Laboratories,. 2016 https://energy.gov/sites/prod/files/2016/06/f32/ace002_busch_2016_o_web.pdf
17. Perini, F., et al., *Piston geometry effects in a light-duty, swirl-supported diesel engine: Flow structure characterization.* International Journal of Engine Research, 2017. **19**(10):1079-1098, https://doi.org/10.1177/1468087417742572
18. Busch, S., Zha, K., Kurtz, E., Warey, A. et al., *Experimental and Numerical Studies of Bowl Geometry Impacts on Thermal Efficiency in a Light-Duty Diesel Engine,* SAE Technical Paper 2018-01-0228, 2018, https://doi.org/10.4271/2018-01-0228
19. Leach, F., et al., *The effect of a stepped lip piston design on performance and emissions from a high-speed diesel engine.* Applied Energy, 2018. **215**:679-689, https://doi.org/10.1016/j.apenergy.2018.02.076
20. Sapio, F., Piano, A., Millo, F., and Pesce, F., *Digital Shaping and Optimization of Fuel Injection Pattern for a Common Rail Automotive Diesel Engine through Numerical Simulation,* SAE Technical Paper 2017-24-0025, 2017, https://doi.org/10.4271/2017-24-0025
21. Ferrari, A., et al., *A new closed-loop control of the injected mass for a full exploitation of digital and continuous injection-rate shaping.* Energy conversion and management, 2018. **177**: 629-639, https://doi.org/10.1016/j.enconman.2018.08.037
22. Ferrari, A. and T. Zhang, *Influence of the injector setup on digital and continuous injection rate-shaping performance in diesel engine passenger cars.* Energy conversion and management, 2020. **205**:112259, https://doi.org/10.1016/j.enconman.2019.112259

23. Payri, R., et al., *Needle lift profile influence on the vapor phase penetration for a prototype diesel direct acting piezoelectric injector.* Fuel, 2013. **113**:257-265, https://doi.org/10.1016/j.fuel.2013.05.057
24. d'Ambrosio, S. and A. Ferrari, *Diesel engines equipped with piezoelectric and solenoid injectors: hydraulic performance of the injectors and comparison of the emissions, noise and fuel consumption.* Applied Energy, 2018. **211**:1324-1342, https://doi.org/10.1016/j.apenergy.2017.11.065
25. Sammut, G., J.S.P. Rodriguez, and S. Ayyapureddi, *Piston for an internal combustion engine*, U.K. Patent GB2580055, 2018, Jaguar Land Rover: UK. https://www.ipo.gov.uk/p-ipsum/Case/PublicationNumber/GB2580055
26. Leach, F., Ismail, R., Davy, M., Weall, A. et al., *Comparing the Effect of Fuel/Air Interactions in a Modern High-Speed Light-Duty Diesel Engine*, SAE Technical Paper 2017-24-0075, 2017, https://doi.org/10.4271/2017-24-0075
27. Papaioannou, N., Leach, F., and Davy, M., *Effect of Thermocouple Size on the Measurement of Exhaust Gas Temperature in Internal Combustion Engines,* SAE Technical Paper 2018-01-1765, 2018, https://doi.org/10.4271/2018-01-1765
28. Papaioannou, N., F. Leach, and M. Davy, *Improving the Uncertainty of Exhaust Gas Temperature Measurements in Internal Combustion Engines.* Journal of Engineering for Gas Turbines and Power, 2020. **142**(7), https://doi.org/10.1115/1.4047283
29. British Standards BS EN 590 *Diesel, Requirements and Test Methods,* 2009. https://knowledge.bsigroup.com/products/automotive-fuels-diesel-requirements-and-test-methods-4
30. Ismail, R., et al., *Computational Investigation of the Effects of Piston Geometry on the Combustion Evolution in a Light Duty HSDI Engine*, in *ASME 2017 Internal Combustion Fall Technical Conference*. ICEF2017-3588, V002T06A014, 2017. ASME: Seattle, WA, USA. https://doi.org/10.1115/ICEF2017-3588